Research Article

Hassan Alzain*, Karim Hussein, Ibrahim Jabr, and Abdullah Alsubaie

Biodegradation of synthetic PVP biofilms using natural materials and nanoparticles

https://doi.org/10.1515/gps-2023-0011 received September 04, 2022; accepted December 19, 2022

Abstract: Biodegradable nanofilms from polyvinyl pyrrolidone (PVP), carboxymethyl cellulose (CMC), citric acid (CA), glycerol (G), and zinc oxide nanoparticles (ZnO-NPs) were prepared using different ZnO concentrations and different electron beam irradiation doses, enabling crosslinking formation. The prepared films were characterized by X-ray diffractometer, Fourier transform infrared spectroscopy, thermogravimetric analyser, and transmission electron microscopy. The swelling percentage of PVP:CMC films was ordered in the sequence of composition ratio 1:2 > 1:1 > 2:1. Results showed decrease in swelling capacity accompanied by increase in gelation percentage of (PVP:CMC)/CA/G)/ZnO nanofilms as the irradiation dose increased up to 20 kGy. The tensile strength of (PVP:CMC) films increased by the incorporation of ZnO-NPs and increasing the irradiation dose. The thermal stability of the prepared (PVP:CMC)/CA/G/ZnO nanofilms was enhanced as the irradiation dosage increased. The water vapour transmission rate of the irradiated films was decreased. The biodegradability of the prepared nanofilms was monitored during 16 weeks and it exceeded 65% weight loss from the original blank weight. Moreover, the nanofilms exhibit antimicrobial activity against fungi, Gram-negative, and Gram-positive bacteria. The broad antimicrobial activity spectrum of the prepared nanofilms increased as the concentration of ZnO-NPs increased. These results suggested that (PVP:CMC)/CA/G/ZnO nanofilms can serve as biodegradable materials in various applications characterized by antimicrobial activity.

Keywords: PVP, CMC, biodegradability, nanofilm, antimicrobial

1 Introduction

Hundred million tons of synthetic plastic are discharged annually directly into the environment without any strategy of degradation [1]. Scientists worldwide have frequently stated that if synthetic materials are not disposed accurately, they will remain throughout the environment ecosystem [2]. According to Mostafa et al., the biodegradation factors of synthetic plastic has to be considered; potential problems can result from the dispersal of different synthetic plastic pollutants throughout our environment. Recently, the introduction of biodegradable plastics as an alternative to synthetic and conventional plastics is in high demand, due to their biocompatibility, biodegradability, and nontoxic characteristics [3]. Biodegradable plastics can be biodegraded by microbial components which already exist in our environment system. Biodegradable type is basically designed using natural materials like proteins and polysaccharides. Many natural biodegradable polymers were used as poly-polyglycolic acid and polylactic acid [4]. Furthermore, the amount of synthetic plastic materials being used determines their potential hazardous and their toxic character, which is considered a potential threat to our environment and also to the human life [5]. There are a few methods for reducing these hazardous wastes from synthetic plastic materials. Some synthetic materials can be degraded in a short time, while others cannot be degraded for a long time, reaching years. For example, biodegradable bags have recently become a market demand. The properties of biodegradable bags are assumed to be similar to conventional synthetic plastic bags [6]. Sometimes biodegradable materials can offer excellent physical properties while being more environmentally eco-friendly.

Biodegradable materials can be prepared from agricultural resources such as vegetable wastes and fruit wastes [7]. Biodegradable plastics can be degraded through anaerobic and aerobic microbial methods. Most researchers have used starch and cellulose films for food safety packaging applications as a proper alternative to the regular polyvinyl alcohol (PVA), polyethylene, and polypropylene food packaging films used due to their advanced environmentally

^{*} Corresponding author: Hassan Alzain, Environmental Protection Organization, Saudi Aramco, Al-Midra Tower, Dhahran 31311, Kingdom of Saudi Arabia, e-mail: Hassan.Alzain@Aramco.com Karim Hussein, Ibrahim Jabr, Abdullah Alsubaie: Environmental Protection Organization, Saudi Aramco, Al-Midra Tower, Dhahran 31311, Kingdom of Saudi Arabia

friendly properties [8–12]. Many other polysaccharides have enhanced properties, such as gas barrier properties and ease of handling, like chitosan and pectin. That describes why the prepared films using these polymers are stable and resistant to oils and fats, also they are antifog, transparent, and flexible [13–15]. The global consumption of biodegradable plastics based on natural polymers has increased 500 times. As a result, massive research is carried on the development of biodegradable polymers to improve the food safety packaging industry [16–18], biomedical applications [19–25], and vehicle industry applications [26]. Generally, natural polymers and biodegradable materials are the future instead of conventional synthetic materials [27–34].

Food packaging materials as a coating form or a membrane form must protect food from contamination through numerous factors which determine the efficiency of packaging materials, such as, gas barrier, permeability, and mechanical strength properties using oil, water, oxygen, and antimicrobial activities. Other factors, such as material costs, recyclability, and disposability, also should be considered [14].

Food deterioration caused by food-borne pathogens and microorganisms are major growing concerns of the food industry. Therefore, a highly encouraging active packaging innovation is antimicrobial packaging system which incorporates antimicrobial agent into a polymer film in order to inhibit bacterial growth, extend the product's shelf life, and enhance food safety [35]. Nanomaterials have a huge impact in food packaging. Incorporation of nano-scaled metal oxides such as zinc oxide (ZnO) within polymeric matrix is of great interest. ZnO is considered as a safe material by Food and Drug Administration (FDA, USA) and has several advantages like low cost, lack of colour, thermal, and chemical stability as well as high antimicrobial activity [36]. ZnO nanoparticles (NPs) are used in drug delivery systems, cosmetics, and food packaging due to their excellent biocompatibility. Notably, they are capable of reducing the oxygen flow inside the packaging containers and act as a barrier against moisture to maintain the food fresh for a prolonged period [37].

A significant number of reports in the literature accounts for the synthesis of ZnO-NPs, with the possibility of tuning their electrical and optical properties for different applications. Among these methods, sol–gel, inert gas condensation, solvo-thermal, chemical precipitation, hydrothermal method, pyrolysis, chemical vapor deposition, laser ablation, and chemical reduction have been used for the production of ZnO-NPs [38]. The biological synthesis of ZnO-NPs through using enzymes, microorganisms, and plants and

their extracts has been suggested as an eco-friendly method for ZnO-NPs synthesis and serves as an alternative to the chemical and physical methods. Various researchers studied the biosynthesis of ZnO-NPs using fungal cultures, date seed extract [39], *Pithecellobium dulce* peel extract [40], *Aegle marmelos* leaves extract [41], *Moringa oleifera* peel extract [42], and goat and sheep faecal matter [43]. Herein, we have used electron beam irradiation technique for the synthesis of ZnO-NPs. Electron beam radiation represents a facile and clean strategy for the synthesis of nanostructured materials without the need for reducing agents and excessive purification steps. In addition, this technique is suitable for the mass production of nanocomposite materials.

The aim of this study is the development of biodegradable nanofilms using cellulose-based materials as a biodegradable component which are more environmentally eco-friendly as an alternative to conventional synthetic plastic materials. The novelty of the current study is the synthesis of ZnO-NPs using electron beam irradiation technique as a clean tool for polymerization, and the preparation of (polyvinyl pyrrolidone [PVP]:carboxymethyl cellulose [CMC])/citric acid (CA)/glycerol (G)/ZnO nanofilms as effective antimicrobial materials for biodegradable packaging applications. Furthermore, the structural, thermal, and surface morphologies of the ZnO-NPs, (PVP:CMC)/CA/G, as well as (PVP:CMC)/CA/G/ZnO nanofilms are characterized. The biodegradation and the antimicrobial activity of these films were investigated by measuring the zone of inhibition of Gram-negative bacteria (Escherichia coli and Pseudomonas aeruginosa), Gram-positive bacteria (Bacillus subtilis and Staphylococcus aureus), and fungus (Candida albicans). To our knowledge, we believe that there is no available data in the literature concerning the effect of different doses of electron beam irradiation, different concentrations of ZnO on mechanical, thermal, biodegradability, and antimicrobial properties of the developed films.

2 Experimental

2.1 Materials

PVP ($M_{\rm w}$ 44 kDa) was purchased from Sigma-Aldrich (Germany), glycerol 99.5% ($M_{\rm w}$ 92.09) was supplied from El-Gomhoria Pharmaceutical Company, Egypt, and CA was purchased from Loba Chemie PVT LTD, Mumbai, India. CMC was used in this study in powder form, and it was purchased from Loba Chemie PVT LTD, Mumbai, India.

2.2 Irradiation technique

Electron beam (EB) irradiation was carried out in ambient air at room temperature using 3 MeV electron energy (energy instability: $\pm 2\%$ maximum), beam current = 30 mA (current instability: ±2% maximum), and beam power = 90 kW EB accelerator. All samples were irradiated using a current of 10 mA and an extraction window length of ≥90 cm; the scan width was controllable from 60 cm up to the maximum width of the scanner. Samples were exposed to irradiation doses of about 2.5, 5, 10, 15, and 20 kGy.

The activation energy was evaluated from the thermogravimetric analyser (TGA) curve based on the Anderson and Freeman method [36], as shown in the following equation:

$$\frac{\log dw/dt}{n \log w^{\circ}} = \frac{E_{a}}{2.203RT} \tag{1}$$

where dw/dt is the rate of thermal decomposition reaction $(mg \cdot min^{-1})$, wo is the reactant mass (mg), R is the gas constant (J·mol⁻¹·K⁻¹), E_a is the energy of activation $(J \cdot mol^{-1})$, and *n* is the order of the reaction. When $\log(dw/dt)$ is plotted against 1/T, and the slope is equal to $E_a/2.303R$, the activation energy can be calculated.

2.3 Swelling percentage

The dried nanofilms of known weight (W_0) were immersed in deionized water for up to 72 h at ambient temperature and reweighed (W_s) after removing the excess water. The swelling percentage was calculated as shown in the following equation:

$$S\% = \frac{Ws - Wo}{Wo} \times 100 \tag{2}$$

2.4 Water vapour transmission rate (WVTR)

Water vapour permeates through a film at a certain temperature and humidity conditions at a steady-state rate. The WVTR was measured gravimetrically at 40°C according to the European Pharmacopeia standard [1,2]. WVTR was represented as the amount of water vapour able to pass through a material, usually within 24 h. The samples were cut into circular samples, each with a diameter of 5 cm, and were placed on the tip, which were made of Teflon material, of a glass bottle containing 50 mL of deionized water. The initial weight was written as W_1 . After a while, the bottles were dried in an oven at 40°C for 24 h. Then, the bottles were taken out, and their weights were recorded as W_2 . The

opened bottle served as a negative control. The percentage of weight loss of the system reflects an index of WVTR. The WVTR was calculated using Eq. 3 and the decrease in WVTR percentage was calculated using Eq. 4 as follows:

WVTR
$$(g \cdot m^{-2}) = \frac{W_1 - W}{A} \times 100$$
 (3)

where A (m²) is the area of film covering the tip of the bottle.

The decrease in WVTR (%)
$$= \frac{WVTR_{negative\ control} - WVTR_{tested\ sample}}{WVTR_{negative\ control}}$$
(4)

2.5 Soil burial biodegradation investigation

The biodegradation study was carried out via a soil burial degradation process conducted at room temperature for 16 weeks. The tested film was the (PVP:CMC)/CA/G/ZnO nanofilm prepared at an irradiation dose of 20 kGy. Sample with a size of $3 \text{ cm} \times 3 \text{ cm}$ was placed in the burial soil at 7 cm depth. The soil composition was moistened with water on a daily basis to overcome water loss by evaporation. Excess water is drained through a hole in the bottom of the pot. The degradation assessment was performed every 2 weeks by taking the sample carefully and washing it with deionized water to remove the residual soil. An oven at a constant 40°C was used to dry the sample until a constant weight. The morphology of the sample after the soil burial process was monitored using a handheld microscope at 200× magnification. The samples' weight loss percentage was determined gravimetrically by recording the weight differences between the samples before and after the burial process. The weight loss percentage was measured weekly during the 16 weeks, and the average weight loss percentage was calculated as the mean of three samples using the following equation:

Weight loss
$$\% = \frac{W_i - W_t}{W_t}$$
 (5)

where W_i (g) is the original weight of the sample and W_t (g) is the weight of the sample at a different point in time after exposure to soil.

2.6 Solubility test

Different solvents such as acetone, ammonia, orthophosphoric acid, methanol, acetic acid, chloroform, sulphuric acid, ethanol, and water were used for samples A, B, and C which were placed into a test tube previously, as shown in Table 1. Then, the solubility of the samples was determined.

was used for the irradiated solution. Then, the precipitated ZnO-NPs were washed with methanol, filtered, and then placed in an oven at 90°C to be dried.

2.7 Preparation of PVP/CMC/ZnO solutions and ZnO-NPs

About 4 g of PVP:CMC mixture was dissolved in 100 mL deionized water at a ratio of 2:1 (PVP:CMC solution). The PVP/CMC solution was then slightly heated to 90°C and continuously stirred using a magnetic stirrer for 8 h (until the polymer solution became completely soluble). Zn (CH₃COO)₂·2H₂O (0.1 M) zinc acetate dihydrate was added with a continuous stirring after the PVP:CMC solution was left to cool at room temperature. Then the isolated ZnO-NPs were extracted from PVP:CMC/ZnO solutions irradiated at 5 kGy. Centrifugation at 15,000 rpm for 30 min

Table 1: Solubility test of the prepared films with different (PVP:CMC) ratios in various solvent media

Solvent	Blend film ratio	Insoluble	Partially soluble	Completely soluble
Methanol	1:1	_	_	_
	1:2	_	\checkmark	_
	2:1	_	\checkmark	_
Acetic acid	1:1	_	\checkmark	_
	1:2	_	\checkmark	_
	2:1	_	_	_
Chloroform	1:1	_	_	
	1:2	_	\checkmark	_
	2:1	_	_	_
Acetone	1:1	_	_	_
	1:2	_	\checkmark	_
	2:1	_	\checkmark	_
Ammonia	1:1	_	_	_
	1:2	_	\checkmark	_
	2:1	_	\checkmark	_
Sulphuric acid	1:1	_	_	_
	1:2	_	\checkmark	_
	2:1	_	\checkmark	
Orthophosphoric	1:1	_	_	_
acid	1:2	_	\checkmark	_
	2:1	_	$\sqrt{}$	_
Ethanol	1:1	_	_	_
	1:2	_	\checkmark	_
	2:1	_	\checkmark	_
Water	1:1	_	_	_
	1:2	_	\checkmark	_
	2:1	-	V	-

2.8 Preparation of blend films and nanofilms

PVP solution of 3 wt% was prepared by dissolving PVP in deionized water at 70°C with continuous stirring until complete dissolution. After that, PVP:CMC films were prepared by mixing the CMC and PVP solutions with different composition ratios of PVP:CMC (V/V: 1/1, 1/2, and 2/1) under continuous and constant stirring at 60°C until the blend changed to a homogenous solution. Then, 0.5 wt% of CA was added to the PVP:CMC mixture, and then 20% v/wt% of glycerol was added as a plasticizer. Finally, the (PVP:CMC)/CA/G mixture solutions underwent electron beam exposure at 2.5, 5, 10, 15, and 20 kGy irradiation doses, and were then cast in Petri dishes and allowed to dry under normal conditions. The (PVP:CMC)/CA/G film with the PVP:CMC composition ratio of 2/1 was selected for the preparation of (PVP:CMC)/CA/G/ZnO nanofilms. This ratio was chosen for its potentially lower swelling value than the other ratios, which makes it the best candidate for the antibacterial and packaging applications. ZnO nanofilms were prepared using the same steps as the fabrication of blend films but using the following amounts of ZnO-NPs: 0.4, 0.6, 0.8, 1, 1.2, and 1.4 wt/wt%. Each value of ZnO was added to a mixture solution of (PVP:CMC)/CA/G and sonicated for 1 h and then stirred for 1 h at 60°C. Then, the (PVP:CMC)/CA/G/ZnO mixture underwent electron beam exposure at 2.5, 5, 10, 15, and 20 kGy irradiation doses, then cast in a Petri dish and left to dry under an ambient atmosphere to form the desired crosslinked film. The suggested reaction mechanisms of formation for the blend film and ZnO nanocomposite films are presented in Figure 1.

2.9 Characterization

The prepared samples' functional groups and chemical structure were determined using an FTIR-Vertex 70 spectrophotometer (Bruker, Karlsruhe, Germany) over $400-4,000\,\mathrm{cm}^{-1}$ spectral range. The crystalline properties of the prepared samples were examined using a fully computerized X-ray diffractometer (XRD, Shimadzu type XD-DI), and the data were recorded for a 2θ angle range of $0-90^\circ$. An X-ray generator was equipped with a scintillation counter at $40\,\mathrm{kV}$ voltage, a filament current of $28\,\mathrm{mA}$, and a scanning speed of

Figure 1: A suggested reactions mechanisms of (PVP:CMC)/CA/G crosslinked film formation and (PVP:CMC)/CA/G/ZnO nanofilm.

20 mm·min⁻¹. Mechanical strength testing was conducted at ambient temperature using an Instron Machine (model 1195, England) of the prepared samples, including elongation and tensile strength with a crosshead speed of 10 mm·min⁻¹ according to ASTM D-638 standards. The values of the elongation and tensile strength at break are reported as the average of five records. Thermal analysis of the films was performed using TGA. The TGA heating rate was 20°C·min⁻¹ up to 600°C, and a flow rate of pure nitrogen of 30 mL·min⁻¹ was used. TGA instrument of (Shimadzu 24 simultaneous DTA-TGA system of type DTG-60 H, Japan). Transmission electron microscopy (TEM, model JEOL JEM-100CX, Japan) adjusted at an acceleration voltage of 80 kV was used to determine the morphology and particle size of ZnO-NPs.

2.10 Bacterial cell growth and viability testing

Bacterial strains were collected from the Italian Hospital in Cairo. For routine use, the cultures were maintained on Luria-Bertani (LB) agar. Glycerol stock solutions were prepared and kept at –20°C for long-term storage. In this study, seven pathogenic microorganisms were selected, including Gram-negative bacterial pathogens (*E. coli* and *P. aeruginosa*), Gram-positive bacterial pathogens (*B. sub-tilis* and *S. aureus*), and a fungus (*C. albicans*). For experimental purposes, bacteria were grown aerobically in 50 mL of LB broth statically at 38°C for 24 h. The overnight culture

of the bacterial suspension (10⁶ CFU·mL⁻¹) was inoculated by spreading on a PVA/PLUR solution containing different fractions of ZnO-NPs. The inhibition zone and monitoring the cell count as a result of the antibacterial properties of the nanofilms were evaluated.

3 Results and discussion

3.1 Solvent solubility study

The solubility data shown in Table 1 show samples treated with water and then chloroform, respectively, and there is an obvious increase in the weight. In contrast, weights declined when samples were treated with methanol, and the plastic property became inelastic. All the prepared samples are convenient in biodegradable polymer preparations; hence, they are totally or partially soluble in the solvents used.

3.2 TEM investigation

TEM was utilized to characterize the morphology and internal structure of the samples. Figure 2a–c displays the TEM images of (PVP:CMC)/CA/G/ZnO nanofilms prepared at irradiation doses from 2.5 to 20 kGy. From Figure 2a–c,

6 — Hassan Alzain et al. DE GRUYTER

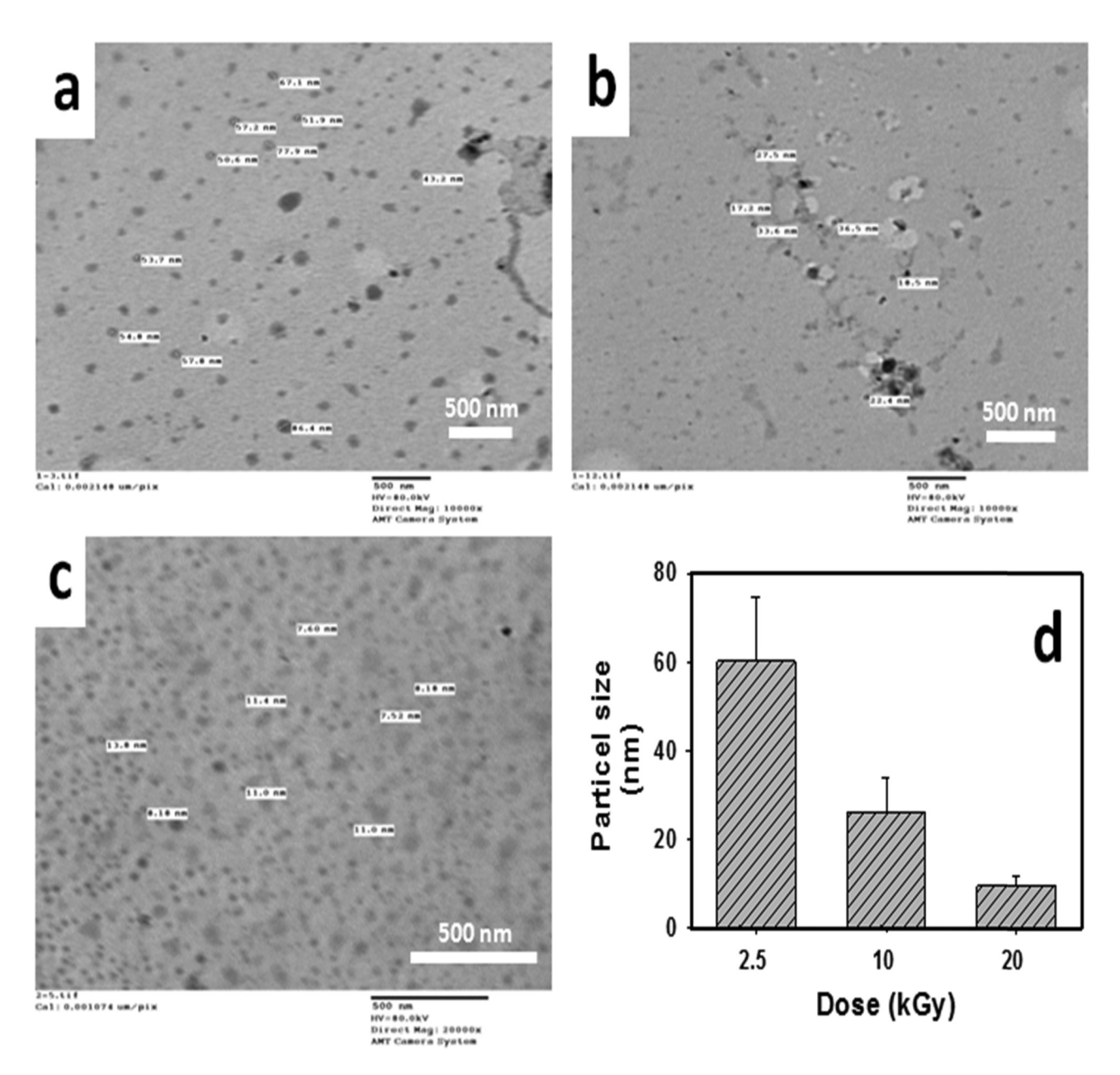


Figure 2: TEM photomicrographs of (PVP:CMC)/CA/G/ZnO nanofilms at: (a) 2.5 kGy, (b) 10 kGy, (c) 20 kGy, and (d) the effect of dose on ZnO-NP size.

all ZnO-NPs look like spheres with good distribution and no aggregation. Moreover, the average nanoparticle size for the prepared samples at 2.5, 10, and 20 kGy is 60 ± 1 , 25 ± 8 , and 9 ± 2 nm, respectively. Figure 2d shows the effect of irradiation dose on the particle sizes. The particle size of ZnO-NPs decreases as the irradiation dose increases which could be attributed to intramolecular hydrogen bonding between the hydroxyl group of CMC and hydrogen as well as the carbonyl group of PVP as shown in Figure 1. These findings are further supported by other investigators who depicted that the irradiation of chitosan led to the

formation of chitosan NPs which decreased in its size with the increase in irradiation dose [44].

3.3 FTIR spectrum

Figure 3a shows the spectrum characteristic peaks of the (PVP:CMC)/CA/G film, which appeared around 1,406 cm⁻¹ and refer to C–H bending and at 2,934 cm⁻¹ corresponding to C–H stretching. The peaks at 1,710 cm⁻¹ correspond to

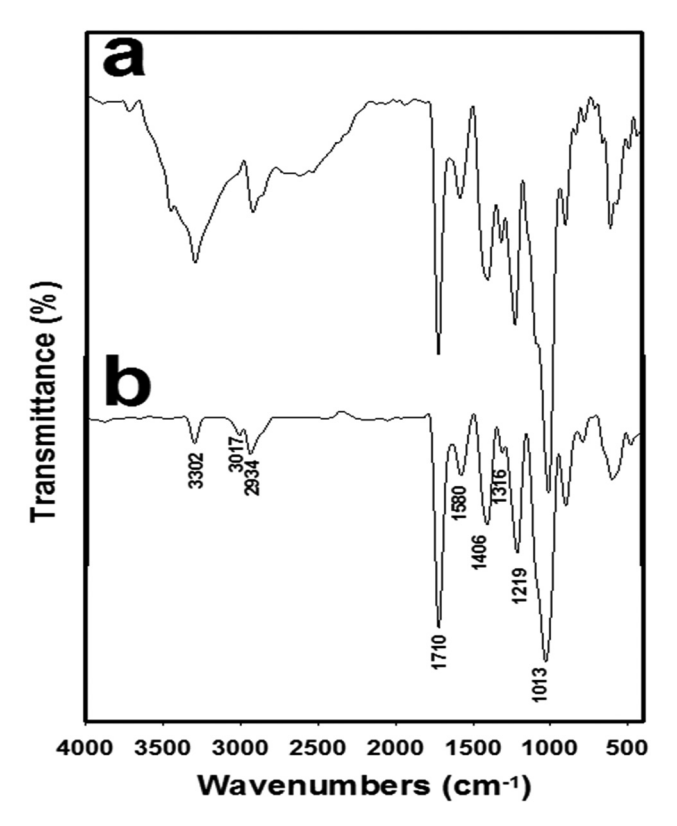


Figure 3: FTIR spectra of (a) (PVP:CMC)/CA/G film and (b) (PVP:CMC)/CA/G-ZnO nanofilm.

carbonyl groups and at 1,580 cm⁻¹ refer to amide group (II) [44]. The ether bridge appears at the peaks in the range of 1,013–1,316 cm⁻¹. Moreover, a broad band of OH groups appeared at 3,302 cm⁻¹. Figure 3b shows the spectrum of the (PVP:CMC)/CA/G/ZnO nanofilm. The significant difference between the (PVP:CMC)/CA/G/ZnO spectra and (PVP:CMC)/CA/G films is the intensity of the peak corresponding to OH groups, which decreased obviously in the presence of ZnO-NPs.

3.4 Swelling study

Figure 4a and b represents the effect of the different irradiation doses on the swelling percentage and the relationship between the swelling percentage and the irradiation dose, respectively. It is seen from Figure 4a that the swelling percentage increases by increasing the time of the immersion process until equilibrium after 3.5 h. However, Figure 4b shows the relationship between the swelling percentage and the irradiation dose at equilibrium. Results reported that the swelling percentage decreases as the irradiation dose increases [45]. This is due to an increment of the crosslinking density that limits the absorption of

water molecules to diffuse among the networks [46]. Further, this relationship is the second regression with a correlation coefficient of $R^2 = 0.99$. The correlation coefficient value reflects the strong connection between the swelling percentage and the irradiation dose.

The swelling character of PVP:CMC films at different composition ratios (V/V) of 1/1, 1/2, and 2/1 is shown in Figure 4c. It was found that the swelling percentage for the PVP:CMC films was directly affected by the change in the composition ratio in the sequence of 1/2 > 1/1 > 2/1. The swelling percentage of PVP:CMC films at composition ratios of 1/2, 1/1, and 2/1 was 406,3%, 231,2%, and 170,4%, respectively, during the first 4h of investigation, and the equilibrium swelling percentage after 24 h was 412.6%, 258.3%, and 173.8%, respectively. The highest increase in swelling percentage of the prepared PVP:CMC film with a composition ratio of 1/1 occurs due to the lower hydrogen bonding formation. As a result, there are lower adhesion forces between PVP and CMC that result in free hydrophilic hydroxyl (OH) groups and carboxylic (COOH) groups of CMC, which leads to a higher swelling percentage due to the existence of internal network spaces. Also, CMC contains the (COOH) group, which establishes an electrostatic force that causes water molecules to diffuse within the blend polymer matrix network. As a result, the swelling percentage was enhanced. In contrast, the increase of the PVP ratio led to a decline in the swelling behaviour, which weakened the relaxation of the intramolecular chains and increased the binding forces by increasing the hydrogen bonding. As a result, less water was allowed to penetrate the prepared film matrix network. Finally, the prepared PVP:CMC film with a composition ratio of 2/1 shows a less swelling percentage, and it was selected for the preparation of (PVP:CMC)/CA/G/ZnO nanofilms. As shown in Figure 4, the swelling percentage for (PVP:CMC)/ZnO nanofilms declined to 20.1% as a result of the increase in the electron beam irradiation dosed and also due to the presence of ZnO-NPs, which are required for packaging purposes. In addition, Figure 4d represents the relationship between the PVP:CMC ratio and swelling percentage. The results represent the ratio of 2/1 for the PVP:CMC blend for the lowest swelling percentage; thus, this value is the best-suited ratio among all the ratios for food packaging applications.

3.5 Effect of different irradiation doses on swelling behaviour

Figure 5 represents the effect of the irradiation dose on the swelling percentage of (PVP:CMC)/CA/G/ZnO nanofilms with a PVP:CMC composition ratio of 2/1 and 1 wt% 8 — Hassan Alzain et al. DE GRUYTER

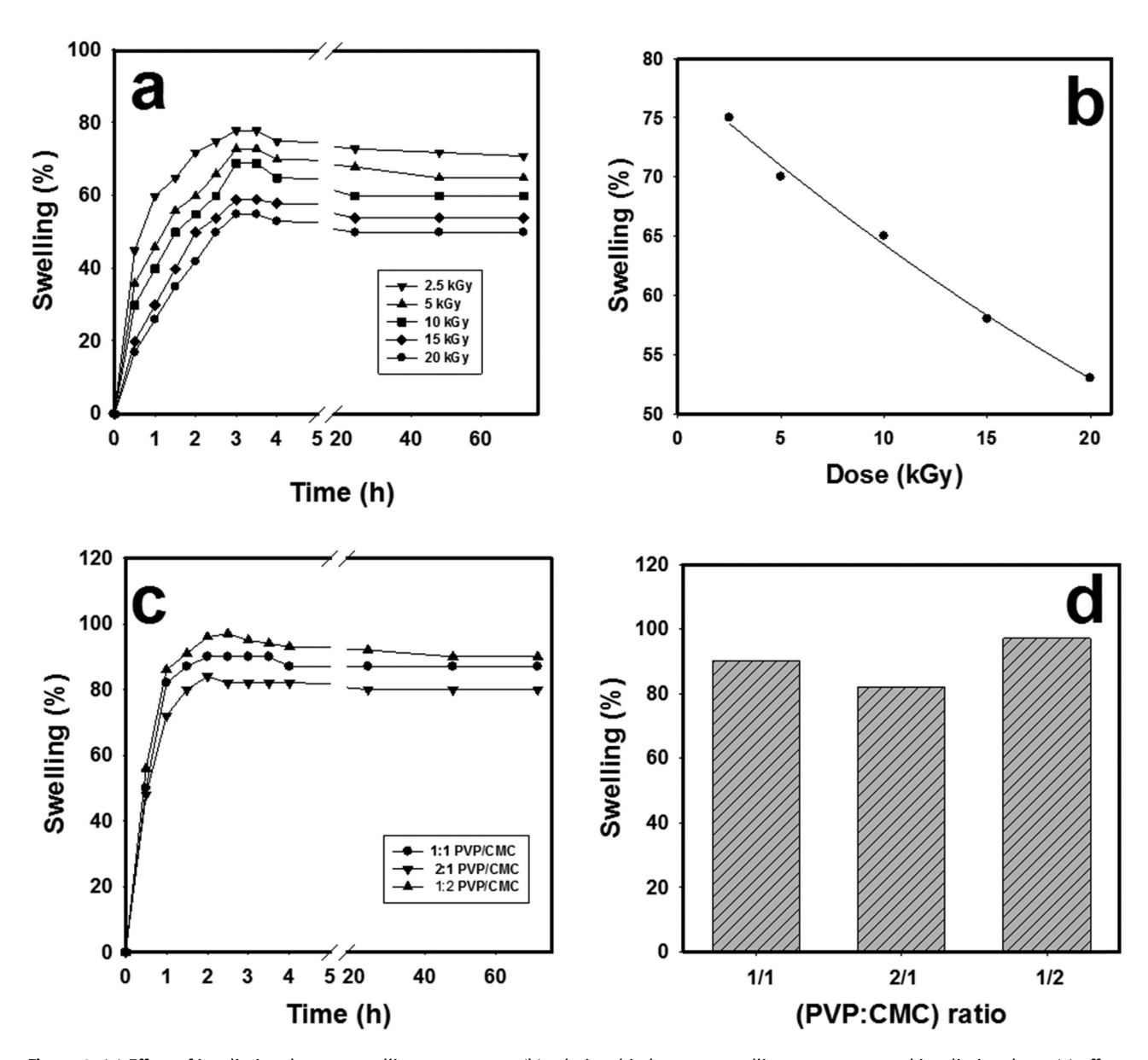


Figure 4: (a) Effect of irradiation dose on swelling percentage, (b) relationship between swelling percentage and irradiation dose, (c) effect of PVP:CMC ratio on swelling percentage, and (d) relationship between swelling percentage and PVP:CMC ratio.

of ZnO-NPs. The results show that the degree of swelling percentage decreased with any increase of the irradiation (from 2.5 to 20 kGy) due to the increase in the crosslinking degree. The swelling percentage at equilibrium for (PVP:CMC)/CA/G)/ZnO nanofilms which irradiated at 2.5, 5, 10, 15, and 20 kGy was found to be decreased, respectively. This decrease in swelling character due to the increase in the irradiation dose can be attributed to the increase in the crosslinking of the PVP:CMC films blended with ZnO. The increase in crosslinking not only reduces the pores and spaces internally between the molecules but also prevents the molecules from stretching and

opening their internal gaps wider, thus resulting in less water being allowed to penetrate the prepared nanofilm matrix.

3.6 Gelation percentage

Figure 6a shows the effect of different irradiation doses on gelation percentage and Figure 6b shows the effect of the (PVP:CMC)/CA/G ratio on gelation percentage, each at 20 kGy. Generally, it is noticed from Figure 6a that by increasing the irradiation dose, the gelation percentage

15

20

2/1

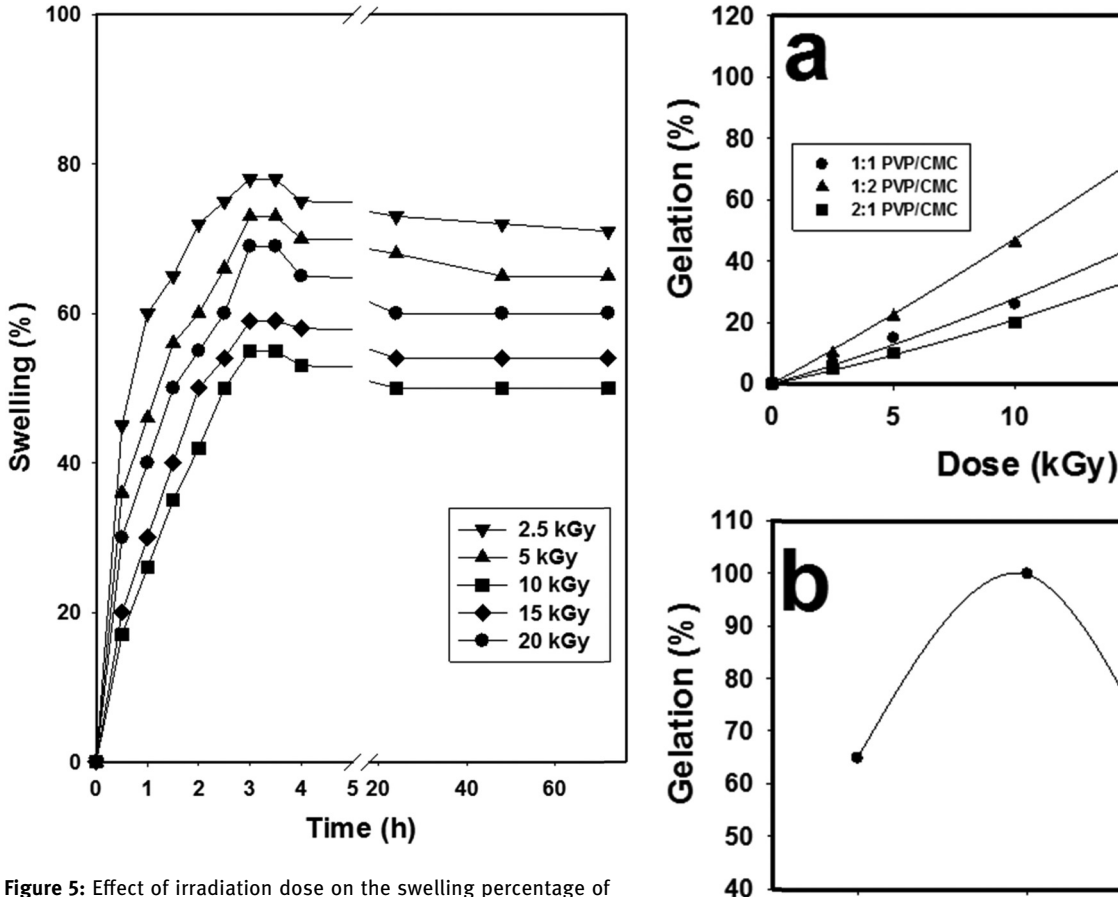


Figure 5: Effect of irradiation dose on the swelling percentage of (PVP:CMC)/CA/G/ZnO nanofilms with a composition ratio of 2/1 and utilizing 1 wt% of ZnO.

increases for three different composition blends. The ratio

of 1/2 for the (PVP:CMC)/CA/G blend demonstrates the highest value of gelation percentage. In contrast, the ratio of 2/1 for the (PVP:CMC)/CA/G blend demonstrates the lowest value of gelation percentage because the gelation formation of PVP has a much higher irradiation dose than that of CMC [47,48]. All data in Figure 6a follow the second regression, with correlation coefficient values ranging between $R^2 = 0.98$ and 0.99. Thus, these values of R^2 represent the direct relationship between the gela-

Moreover, Figure 6b shows the relationship between the (PVP:CMC)/CA/G composition blend and the gelation percentage. The results represent that the presence of PVP in the *in situ* polymerization mixture limits the value of the gelation percentage. The feeding solution composition at 2/1 of PVP:CMC shows a gelation percentage of less than 50%. In contrast, the feeding solution compositions at 1/1 and 1/2 show that the values of gelation percentage are more than 60% and 100%, respectively.

tion percentage and irradiation dose, and obviously, it

was intense.

Figure 6: (a) Effect of irradiation dose on the gelation percentage and (b) effect of PVP:CMC ratio on gelation percentage at 20 kGy.

1/2

(PVP/CMC) ratio

3.7 Mechanical properties

1/1

Mechanical characters are a vital property of the prepared films being used in food packaging applications. Figure 7a and b describes the effect of different irradiation doses on the mechanical properties, elongation percentage, and tensile strength of PVP:CMC prepared film with a composition ratio of 2/1. Figure 7a and b shows that the higher PVP content in the prepared films results in higher, softer, and more elastic mechanical properties. It is widely known that CMC is very brittle to form a thin film, and PVP films dissolve easily in water [49,50]. The mechanical properties of the prepared PVP:CMC films were improved by using electron beam irradiation exposure. Figure 7a represents the effect of irradiation doses on the tensile strength of the prepared PVP:CMC film, which increased clearly as the irradiation dose was increased up to 20 kGy. Also, Figure 7b shows the effect 10 — Hassan Alzain et al. DE GRUYTER

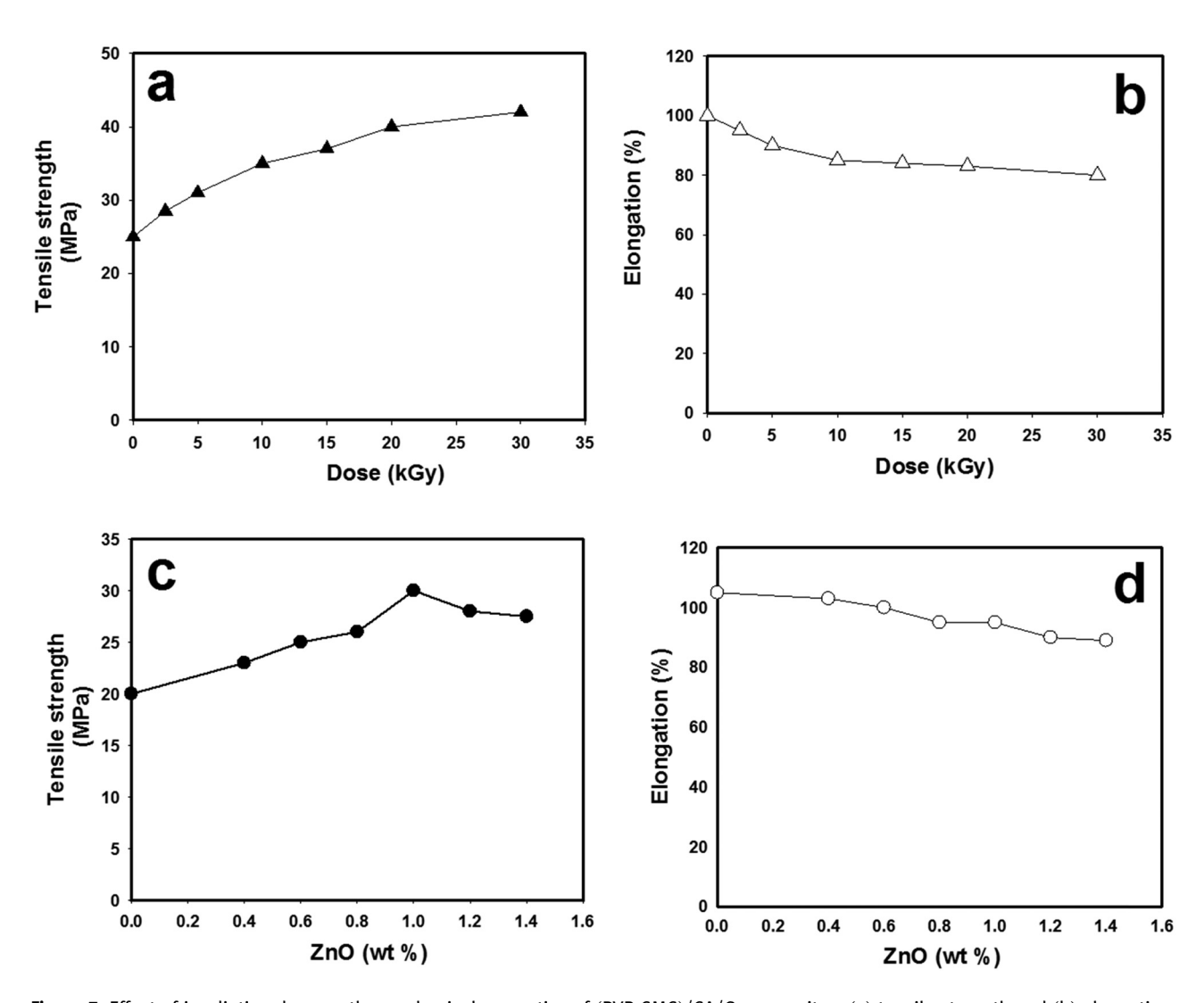


Figure 7: Effect of irradiation dose on the mechanical properties of (PVP:CMC)/CA/G composites: (a) tensile strength and (b) elongation percentage. Effect of ZnO-NPs concentration on the mechanical properties of (PVP:CMC)/CA/G/ZnO nanofilms: (c) tensile strength and (d) elongation.

of electron beam irradiation dosage on the elongation at break percentage of the prepared PVP:CMC film. It is noticed that no changes were obtained at an irradiation dose of 20 kGy. The interfacial bonds between PVP and CMC were increased that form crosslinked structures and increases the adhesion force between PVP and CMC via electron beam irradiation doses [51].

On the other hand, the effect of ZnO-NP contents on elongation percentage and tensile strength property at the break for (PVP:CMC)/CA/G/ZnO nanofilms irradiated at 20 kGy is represented in Figure 7c and d. It was noticed that as ZnO-NP contents increased up to 1 wt%, the tensile strength property increased; then, the tensile strength property decreased as the ZnO-NP contents increased up to 1.4 wt%. Generally, adding ZnO-NPs into the PVP:CMC

polymer blend mixture increases the tensile strength of the nanofilm, as represented in Figure 7c. This is due to the interaction between the gel-formed networks and ZnO-NPs with a high surface area, forming a strong interfacial adhesion bond between them. The interfacial adhesion interaction between the intramolecular network and fillers directly affect the mechanical properties of the prepared nanofilms [52]. It was reported that no remarkable change occurred in the elongation property at break percentage with the incorporation of ZnO-NPs up to 1.0 wt%, as represented in Figure 7d. Therefore, the existence of ZnO-NPs in the films' composition remarkably enhance the mechanical properties of the prepared (PVP:CMC)/CA/G/ZnO nanofilm. The optimum results of elongation properties and tensile strength at the broken

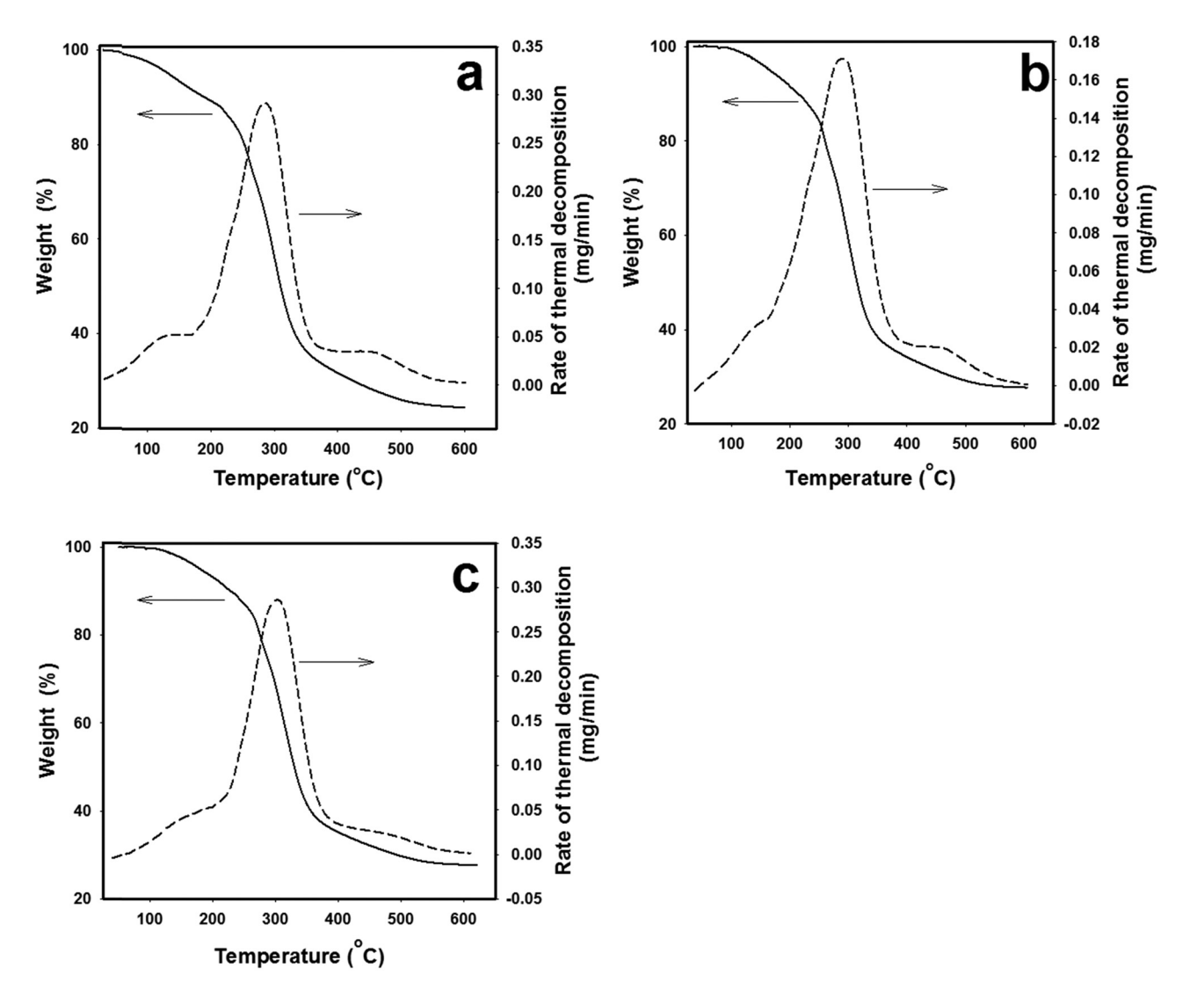


Figure 8: TGA curves of (a) PVP/CMC film (2/1), (b) (PVP:CMC)/ZnO nanofilm irradiated at 5 kGy, and (c) (PVP:CMC)/ZnO nanofilm irradiated at 20 kGy PVP:CMC with a particular PVP:CMC ratio (2/1) and ZnO content (1.2 wt%).

percentage of (PVP:CMC)/CA/G ZnO-NPs nanofilm were found at 1 wt% of ZnO nanoparticle contents.

3.8 TGA investigation

Figure 8 represents the TGA thermographs of PVP:CMC films and (PVP:CMC)/ZnO nanofilms which are irradiated at 5 and 20 kGy and has been investigated within 25°C and 600°C temperature range as a function of the weight loss percentage. The weight loss percentage at different temperature degrees, the decomposition stages at different temperature ranges and their temperature for maximum rate of decomposition ($T_{\rm max}$) for each stage, and the activation energies (Ea) (kJ·mol $^{-1}$) are reported in Table 2. The thermal decomposition of the prepared

PVP:CMC blend film (Figure 8a) represented three main weight loss stages.

Initial stage was in the range of 43–165°C with 3.5% weight loss due to moisture vaporization. Second stage occurred in range of 165–425°C ($T_{\rm max}$ 287°C) with 75.5% weight loss due to the decomposition of intermolecular crosslinking of the PVP and CMC chains inside the formed polymer. The third stage occurred at 425–595°C and is due to the carbonization and the breakage of the C–C backbone of the polymer chains, leaving 2.5% as a residual substance.

The thermal decomposition of (PVP:CMC)/ZnO nanofilms, which were irradiated at 5 (Figure 8b) and 20 kGy (Figure 8c) showed three decomposition stages. The first stage of weight loss happened in the ranges of 44–165°C and 45–167°C ($T_{\rm max}$ 156°C), respectively, with a weight

Table 2: Weight loss of samples A, B, and C at different temperatures

Sample number	Dose (kGy)	Weight loss percentage at various temperatures						T_{max}	$E_a (kJ \cdot mol^{-1})$
		100°C	200°C	300°C	400°C	500°C	600°C		
A	0	2.7	10.9	44.3	68.2	74.1	75.5	287	38.78
В	5	0.95	8.73	41.92	65.8	71	72.9	293	55.57
C	20	0.2	7.3	31.74	65.3	70.7	72.4	304	67.14

loss of 3%, caused by the loss of physically adsorbed water and hydrogen-bonded water. The second stage occurred in the ranges of 165-425°C (T_{max} 293°C) and 165-425°C (T_{max} 304°C), with a weight loss of 65.7%, resulting from the decomposition of intermolecular crosslinking of CMC and PVP chains inside the formed polymers with a further decomposition of the backbone of the formed polymers to carbon and hydrocarbon substances. PVP and CMC contain many hydrophilic hydroxyl groups, and the intermolecular and intramolecular hydroxyl groups are attached easily and form hydrogen bonds. Breakage of the C-C bond of the main backbone of the prepared happened in the third stage in the range of 425–598°C with 72% weight loss and this is what scientists called as carbonization process [53]. At the end of the test, all contents of CMC and PVP in nanofilms which were irradiated at 5 and 20 kGy were digested, leaving 6.5% and 10.5% as a residue of the ZnO-NPs content.

The activation energies of (PVP:CMC)/CA/G and (PVP:CMC)/CA/G/ZnO nanofilms which irradiated at 5 and 20 kGy were 38.78, 55.57, and $67.14 \text{ kJ} \cdot \text{mol}^{-1}$, respectively. The activation energies of the prepared (PVP:CMC)/CA/G/ZnO nanofilms were found to be higher than that of the prepared (PVP:CMC)/CA/G films. The activation energy of the nanofilms increased as the irradiation dose increased. Higher activation energy corresponds to a tremendous amount of energy required to degrade the higher molecular weight of polymeric chains. This is due to high temperatures, and the formation of a stable complex might be due to the presence of ZnO-NPs; hence, more energy was needed to cleavage the complex. It was noticed that the thermal stability of the prepared (PVP:CMC)/CA/G/ZnO nanofilms was better than that of the prepared PVP:CMC blend films. The addition of ZnO-NPs has considerable effects on the thermal stability of the nanofilms. This thermal stability enhancement can be attributed to an improvement in the interfacial adhesion bonds and compatibility between the ZnO-NPs and PVP:CMC polymer matrix. Moreover, the thermal stability of the prepared (PVP:CMC)/CA/G/ZnO nanofilms was enhanced as the irradiation dosage increased. This is because increasing the crosslinking percentage by irradiation dose

will limit the chains' mobility between PVP:CMC and ZnO-NPs network in the formation of the nanofilms, improving the thermal stability at the higher dosage of 20 kGy.

3.9 Water vapour permeability

WVTR is an essential factor in film preparations for food packaging materials and widely determines their ability to maintain the quality of the products. The WVTR was determined gravimetrically and expressed as the amount of water vapour in grams that could pass through the prepared material within 24 h. The WVTR values of the prepared films are shown in Figure 9. The WVTR of the prepared (PVP:CMC)/CA/G/ZnO nanofilms was lower with a remarkable difference when compared with the prepared (PVP:CMC)/CA/G blend films in the presence of negative control (uncoated or opened bottle). The addition of ZnO-NPs into (PVP:CMC)/CA/G films represented a decrease in the WVTR values. This is due to the formation of a denser polymer structure in the (PVP:CMC)/CA/G/ZnO nanofilms compared to the unfilled films. Also, adding ZnO-NPs to the prepared film could produce a more complex network path, prolonging water vapour molecules' transport [54]. When comparing the decrease in WVTR percentage with the uncoated bottle (negative control), the WVTR of the (PVP:CMC)/CA/G film showed approximately 37.3% lower value.

Meanwhile, the decreased WVTR of the prepared (PVP:CMC)/CA/G/ZnO nanofilms irradiated at 5, 10, 15, and 20 kGy was 62.4%, 67.2%, 75.6%, 81.2%, and 86.3%, respectively. As the irradiation dose increased, the WVTR percentage decreased due to increased crosslinking between polymer chains and, therefore, less permeability of water vapour molecules.

3.10 Biodegradation

The biodegradability of polymers is critical to their possible applications. Using biodegradable food packaging

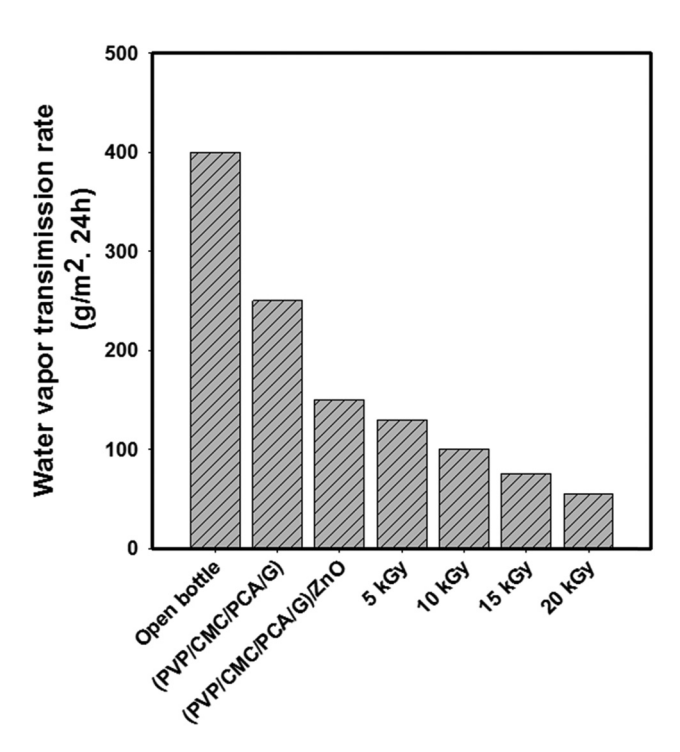


Figure 9: WVTR of the open bottle, (PVP:CMC)/CA/G film, and (PVP:CMC)/CA/G/ZnO nanofilms irradiated at 5, 10, 15, and 20 kGy, respectively.

materials is considered an intelligent solution for solid waste accumulation and environmental problems. The biodegradability of the prepared (PVP:CMC)/CA/G/ZnO nanofilms was studied using the burial degradation process by evaluating the weight loss percentage over time for 16 weeks, as represented in Figure 10a. The weight loss records are essential to check the biodegradation character and the degradation rate of polymeric materials during the soil burial process. The weight loss percentage of the prepared nanofilms represented a recorded degradation, and the degradation rate increased obviously in the initial 10 weeks. After that, the biodegradation process continued at a significant slower rate. After 16 weeks, weight loss percentage of the tested sample was 61%. In addition, both CMC and PVP are hydrophilic and partially degraded products that would also contribute to the weight loss of the prepared film. During CMC degradation, the moisture content is the primary action of the degradation process. It involves water absorption, ester breakage forming oligomers, solubilization of oligomer fractions, and diffusion of soluble oligomers by bacteria [52]. It is proposed that two stages of degradation take place in the soil burial process: (1) the diffusion of water into the prepared film matrix samples results in the swelling of the film's network and allows the growth of microorganisms on the film's threads and (2) enzymatic degradation and

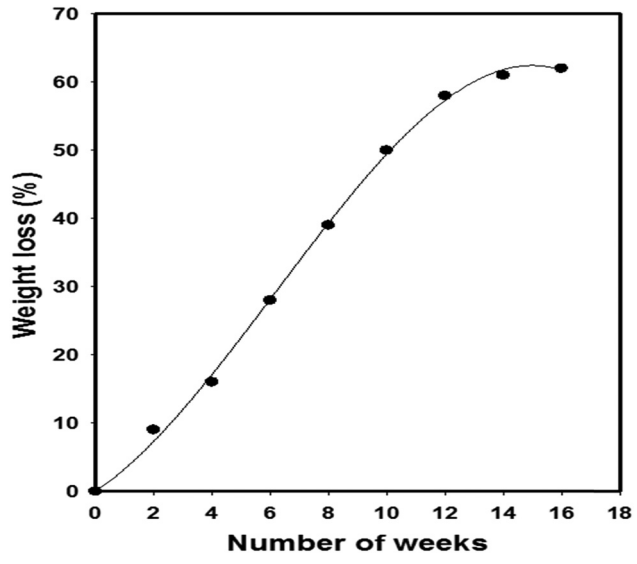


Figure 10: Biodegradability of (PVP:CMC)/CA/G/ZnO nanofilm over 16 weeks.

other types of degradation cause weight loss and deterioration of the film samples. It was reported that the colour of the prepared nanofilms changed from white to yellow within the first 4 weeks of the burial process. After that, the colour changed to reddish brown. These results match with several other studies which reported the biodegradation of the prepared CMC composites [55,56]. The weight loss of the biodegradable nanofilm and the time of biodegradation undergo the second regression relationship and exhibit a correlation coefficient of $R^2 = 0.98$. Hence, the value of R^2 expresses the strong relationship between the time of biodegradation and the weight loss value.

3.11 Antimicrobial activity

Metal NPs embedded biopolymers have been shown to have effective antimicrobial activity due to their novel property of surface area to the volume ratio, which enhances the combination of many ligands on their surfaces. These nanocomposites exhibited effective antibacterial activity in many studies. Substantial antibacterial activities of copper oxide NPs and silver chloride NPs have been reported [57,58]. Authors of ref. [59] represented that copper oxide nanocomposites demonstrated great antifungal activity which mediated through cell membrane disruption and mitochondrial damage. Additionally, ZnO-NPs have represented outstanding antimicrobial activities and have been used in various applications for food protection membranes [56]. This study incorporated ZnO-NPs into

Table 3: Influence of different concentrations of ZnO-NPs in the matrix of (PVP:CMC)/CA/G films on the growth of different microbial strains

Strains	Inhibition zone (mm)						
	0.4 wt%	0.6 wt%	0.8 wt%	1 wt%	1.2 wt%	1.4 wt%	
E. coli	5 ± 0.1	6 ± 0.2	6 ± 0.1	10 ± 0.4	14 ± 0.2	18 ± 0.2	
B. subtilis	10 ± 0.2	10 ± 0.1	13 ± 0.2	16 ± 0.2	19 ± 0.1	20 ± 0.1	
C. albicans	20 ± 0.1	22 ± 0.3	25 ± 0.2	27 ± 0.1	35 ± 0.1	38 ± 0.1	
P. aeruginosa	10 ± 0.2	12 ± 0.1	16 ± 0.2	20 ± 0.2	26 ± 0.4	30 ± 0.2	
S. aureus	18 ± 0.1	18 ± 0.2	26 ± 0.1	29 ± 0.1	32 ± 0.1	36 ± 0.1	

All values of data are mean \pm SD (n = 3).

the blank (PVP:CMC)/CA/G films to enhance their antimicrobial activity. The prepared (PVP:CMC)/CA/G/ZnO nanofilms were used as dual function materials for food packaging with antimicrobial effects. This study reports the enhanced activity of the biodegradable (PVP:CMC)/CA/G/ZnO nanofilms as antimicrobial against foodborne pathogens, especially *E. coli* [60]. This pathogen causes colon inflammation, leading to diarrhoea and abdominal pain with blood in stools. The effect of different concentrations of ZnO-NPs (0.4, 0.6, 0.8, 1, 1.2, and 1.4 wt%) was determined by measuring the inhibition zone against pathogenic Gram-negative (*E. coli* and *P. aeruginosa*) strains, Gram-positive (*B. subtilis* and *S. aureus*), and fungus (*C. albicans*).

Results in Table 3 show that antimicrobial activity can be seen against all strains understudying all ZnO-NP concentrations, with inhibition zone values from 5 to 35 mm in diameter. The most vigorous activity was reported against *C. albicans* (38 mm) and *S. aureus* (36 mm). The weakest growth inhibition was against *E. coli* (18 mm).

4 Conclusion

Biodegradable films and nanofilms were prepared from PVP, CMC, CA, glycerol, and ZnO-NPs. These nanofilms were prepared at different concentrations of ZnO-NPs and at various electron beam irradiation doses. Nanofilms were characterized by TEM, FTIR, XRD, and TGA. The swelling study was conducted at different concentrations of ZnO-NPs and different compositions of PVP and CMC in the *in situ* media copolymerization reaction, and the activation energy of the prepared films was determined. In addition, the WVTR was evaluated for polymer blend films, ZnO nanofilms, and irradiated films at different irradiation doses. The biodegradability of nanofilms was investigated during 16 weeks. The biodegradability of films exceeded 65% as weight loss from the original weight. Moreover, (PVP:CMC)/CA/G/ZnO nanofilms have an antimicrobial activity

against negative bacterial pathogens, Gram-positive, and fungi, with a broad-spectrum. As the concentrations of ZnO-NPs increased the antimicrobial activity increased. These results suggest that (PVP:CMC)/CA/G/ZnO nanofilms are effective antimicrobial materials for biodegradable food-packaging applications.

Funding information: Authors state no funding involved.

Author contributions: Hassan Alzain, Karim Hussein, Ibrahim Jabr, and Abdullah Alsubaie designed the study along with carrying out the research and writing the article.

Conflict of interest: The authors of this article are solely responsible for the content thereof. Data, ideas, and opinions presented herein do not necessarily represent the corporate views of the Saudi Arabian Oil Company.

References

- [1] Ogunola OS, Onada OA, Falaye AE. Mitigation measures to avert the impacts of plastics and microplastics in the marine environment (a review). Environ Sci Pollut Res. 2018;25:9293–310.
- [2] STompson R, Moore C, Andrady A, Gregory M, Takada H, Weisberg S. New directions in plastic debris. Science. 2005;310:1117–18.
- [3] Mostafa YS, Alrumman SA, Alamri SA, Otaif KA, Mostafa MS, Alfaify AM. Bioplastic (poly-3-hydroxybutyrate) production by the marine bacterium *Pseudodonghicola xiamenensis* through date syrup valorization and structural assessment of the biopolymer. Sci Rep. 2020;10:1–13.
- [4] Yaradoddi JS, Banapurmath NR, Ganachari SV, Soudagar MEM, Mubarak NM, Hallad S, et al. Biodegradable carboxymethyl cellulose-based material for sustainable packaging application. Sci Rep. 2020;10:21960. doi: 10.1038/s41598-020-78912-z.
- [5] Gerritse J, Leslie HA, Caroline A, Devriese LI, Vethaak AD. Fragmentation of plastic objects in a laboratory seawater microcosm. Sci Rep. 2020;10:1–16.

- [6] Fernández-Braña Á, Feijoo-Costa G, Dias-Ferreira C. Looking beyond the banning of lightweight bags: analyzing the role of plastic (and fuel) impacts in waste collection at a Portuguese city. Environ Sci Pollut Res. 2019;26:35629–47.
- [7] Yaradoddi JS, Hugar S, Banapurmath NR, Hunashyal AM, Sulochana MB, Shettar AS, et al. Alternative and renewable bio-based and biodegradable plastics. In: Martinez LMT, Kharissova OV, Kharisov BI, editors. Handbook of eco-materials. Cham: Springer; 2019.
- [8] Bonilla J, Talón E, Atarés L, Vargas M, Chiral A. Effect of the incorporation of antioxidants on physicochemical and antioxidant properties of wheat starch-chitosan films. J Food Eng. 2013;118:271-8.
- [9] Campos CA, Gerschenso LN, Flores SK. Development of edible films and coatings with anti-microbial activity. Food Bioprocess Technol. 2011;4:849-75.
- [10] Mali S, Grossmann MVE, García MA, Martino MN, Zaritzky NE. Barrier, mechanical and optical properties of plasticized yam starch films. Carbohydr Polym. 2004;56(129):135–5.
- [11] Versino F, Lopez OV, Garcia MA, Zaritzky NE. Starch-based films and food coatings: an overview. Starch-Stärke. 2016;68:1026-37.
- [12] Taranathan R. Biodegradable films and composite coatings: past, present and future. Trends Food Sci Technol. 2003;14:71–8.
- [13] Vieira M, da Silva MA, dos Santos LO, Beppu MM. Naturalbased plasticizers and biopolymer films: a review. Eur Polym J. 2011;47:254-63.
- [14] Jacob J, Loganathan S, Tomas S. Chitin- and chitosan-based biocomposites for food packaging applications. Boca Raton: CRC Press; 2020.
- [15] Attaran SA, Hassan A, Wahit MU. Materials for food packaging applications based on bio-based polymer nanocomposites: a review. J Thermoplast Compos Mater. 2017;30:143-73.
- [16] Youssef AM, El-Sayed SM, Salama HH, El-Sayed HS, Dufresne A. Evaluation of bionanocomposites as packaging material on properties of white cheese during storage period. Carbohydr Polym. 2015;132:274–85.
- [17] Tomas S, Mishra RK, Asiri AM. Sustainable polymer composites and nanocomposites. Berlin: Springer; 2019.
- [18] Pérez-Gómez EO, Cruz GJ, García-Rosales G, Serafín-Díaz K, Mejía MdR, González-Torres M, et al. Synthesis by plasma of potentially biodegradable oxidized polyethylene obtained from ethanol. Polym Bull. 2020;77:6017–27. doi: 10.1007/ s00289-019-03063-9.
- [19] Mondal S. Preparation, properties and applications of nano cellulosic materials. Carbohydr Polym. 2017;163:301–16.
- [20] Safari R, Lopresti F, D'Arrigo M, Marino A, Nostro A. Efficacy of poly(lactic acid)/carvacrol electrospun membranes against Staphylococcus aureus and Candida albicans in single and mixed cultures. Appl Microbiol Biotechnol. 2018;102:4171–81.
- [21] Sittipummongkol K, Chuysinuan P, Techasakul S, Pisitsak P, Pechyen C. Core-shell microcapsules of neem seed oil extract containing azadirachtin and biodegradable polymers and their release characteristics. Polym Bull. 2019;76:3803-17.
- [22] Prajapati SK, Jain A, Jain A, Jain S. Biodegradable polymers and constructs: a novel approach in drug delivery. Eur Polym J. 2019;120:109-91.
- [23] Koc FE, Altıncekic TG. Investigation of gelatin/chitosan as potential biodegradable polymer films on swelling behavior and methylene blue release kinetics. Polym Bull. 2020;78:3383–98. doi: 10.1007/s00289-020-03280-7.

- [24] Francisco W, Ferreira FV, Ferreira EV, Cividanes LeS, Coutinho AdR, Thim GP. Functionalization of multi-walled carbon nanotube and mechanical property of epoxy-based nanocomposite. J Aerosp Technol Manag. 2015;7:289-93.
- [25] Naskar AK, Keum JK, Boeman RG. Polymer matrix nanocomposites for automotive structural components. Nat Nanotechnol. 2016;11:1026-30.
- [26] Kargarzadeh H, Mariano M, Huang J, Lin N, Ahmad I, Dufresne A, et al. Recent developments on nanocellulose reinforced polymer nanocomposites: a review. Polymer. 2017;132:368–93.
- [27] Patil AY, Banapurmath NR, Yaradoddi JS, Kotturshettar BB, Shettar AS, Basavaraj GD, et al. Experimental and simulation studies on waste vegetable peels as bio-composite fillers for light duty applications. Arab J Eng Sci. 2019;44:7895-07.
- [28] Pfaendner R. Nanocomposites: industrial opportunity or challenge? Polym Degrad Stab. 2010;95:369-73.
- [29] Cerruti P, Santagata G, Gomez d'Ayala G, Ambrogi V, Carfagna C, Malinconico M, et al. Effect of a natural polyphenolic extract on the properties of a biodegradable starchbased polymer. Polym Degrad Stab. 2011;96:839-46.
- [30] Moreno O, Atarés L, Chiral A. Effect of the incorporation of antimicrobial/antioxidant proteins on the properties of potato starch films. Carbohydr Polym. 2015;133:353-64.
- [31] Pelissari FM, Grossmann MV, Yamashita F, Pineda EAG. Anti-microbial, mechanical, and barrier properties of cassava starch-chitosan films incorporated with oregano essential oil. J Agric Food Chem. 2009;57:7499-504.
- [32] Engel JB, Ambrosi A, Tessaro IC. Development of biodegradable starch-based foams incorporated with grape stalks for food packaging. Carbohydr Polym. 2019;225:115–234.
- [33] Shellikeri A, Kaulgud V, Yaradoddi J, Ganachari Sh, Banapurmath N, Shettar A. IOP Conference Series: Materials Science and Engineering, Proceedings of International Conference on Advances in Manufacturing, Materials and Energy Engineering (ICon MMEE 2018), Mangalore Institute of Technology & Engineering, Badaga Mijar, Moodbidri, Karnataka, India, 2018. p. 2–3.
- [34] Tamayo L, Azócar M, Kogan M, Riveros A, Páez M. Copperpolymer nanocomposites: an excellent and cost-effective biocide for use on antibacterial surfaces. Mater Sci Eng C. 2016;69:1391–409.
- [35] Sung S-Y, Sin LT, Tee T-T, Bee S-T, Rahmat AR, Rahman WAWA, et al. Antimicrobial agents for food packaging applications. Trends Food Sci Technol. 2013;33(2):110-23.
- [36] Kim I, Viswanathan K, Kasi, Sarinthip G, Kambiz S, Jongchul S. ZnO nanostructures in active antibacterial food packaging: preparation methods, antimicrobial mechanisms, safety issues, future prospects, and challenges. Food Rev Int. 2022;38(4):537-65. doi: 10.1080/87559129.2020.1737709.
- [37] Huang Y, Mei L, Chen X, Wang Q. Recent developments in food packaging based on nanomaterials. Nanomaterials. 2018;8:830. doi: 10.3390/nano8100830.
- [38] Perveen R, Shujaat S, Qureshi Z, Nawaz S, Khan MI, Iqbal M. Green versus sol-gel synthesis of ZnO nanoparticles and antimicrobial activity evaluation against panel of pathogens. J Mater Res Technol. 2020;9(4):7817-27.
- [39] El-Naggar NEA, Hussein MH, El-Sawah AA. Bio-fabrication of silver nanoparticles by phycocyanin, characterization, in vitro anticancer activity against breast cancer cell line and in vivo cytotoxicity. Sci Rep. 2017;7:10844. doi: 10.1038/s41598-017-11121-3.

- [40] Madhumitha G, Fowsiya J, Gupta N, Kumar A, Singh M. Green synthesis, characterization and antifungal and photocatalytic activity of *Pithecellobium dulce* peel-mediated ZnO nanoparticles. J Phys Chem Solids. 2019;127:43-51.
- [41] Fowsiya J, Asharani IV, Mohapatra S, Eshapula A, Mohi P, Thakar N, et al. *Aegle marmelos* phytochemical stabilized synthesis and characterization of ZnO nanoparticles and their role against agriculture and food pathogen. Green Process Synth. 2019;8(1):488–95. doi: 10.1515/gps-2019-0017.
- [42] Surendra TV, Roopan SM, Al-Dhabi NA, Arasu MV, Sarkar G, Suthindhiran K. Vegetable peel waste for the production of ZnO nanoparticles and its toxicological efficiency, antifungal, hemolytic, and antibacterial activities. Nanoscale Res Lett. 2016:11:546. doi: 10.1186/s11671-016-1750-9.
- [43] Chikkanna MM, Neelagund SE, Rajashekarappa KK. Green synthesis of zinc oxide nanoparticles (ZnO NPs) and their biological activity. SN Appl Sci. 2019;1:117. doi: 10.1007/ s42452-018-0095-7.
- [44] Radwan RR, Ali HE. Radiation-synthesis of chitosan/poly (acrylic acid) nanogel for improving the antitumor potential of rutin in hepatocellular carcinoma. Drug Deliv Transl Res. 2021;11:261–78. doi: 10.1007/s13346-020-00792-7.
- [45] Yacob N, Hashim K. Morphological effect on swelling behaviour of hydrogel. AIP Conf Proc. 2014;1584:153-9. doi: 10.1063/1.4866123.
- [46] Mahkam M, Dostie L. The relation between swelling properties and crosslinking of hydrogels designed for colon-specific drug delivery. Drug Deliv. 2005;12(6):343–47. doi: 10.1080/ 10717540590952627.
- [47] Oliveira MJ. Effect of gamma radiation on polyvinylpyrrolidone hydrogels. Conference: International Nuclear Atlantic Conference – INAC. Belo Horizonte, MG, Brazil: 2017.
- [48] Liu P, Peng J, Li J, Wu J. Radiation crosslinking of CMC-Na at low dose and its application as substitute for hydrogel. Rad Phys Chem. 2005;72:635–8. doi: 10.1016/j.radphyschem.2004. 03.090.
- [49] Eom Y, Choi B, Park SI. A study on mechanical and thermal properties of PLA/PEO blend. J Polym Environ. 2019;27:256–62.

- [50] Tang X, Alavi S. Recent advances in starch, polyvinyl alcohol based polymer blends, nanocomposites and their biodegradability. Carbohydr Polym. 2011;85:7–16.
- [51] Ghaffar AMA, Ali HE. Radiation modification of the properties of polypropylene/carboxymethyl cellulose blends and their biodegradability. Bull Mater Sci. 2016;39:1809-17.
- [52] Ma X, Chang PR, Yang J, Yu J. Preparation and properties of glycerol plasticized-pea starch/zinc oxide-starch bionanocomposites. Carbohydr Polym. 2009;75:472–8.
- [53] Yang L, Zhang HY, Yang Q, Lu DJ. Bacterial cellulose-poly(vinyl alcohol) nanocomposite hydrogels prepared by chemical crosslinking. Appl Polym Sci. 2012;126:E245-51.
- [54] Kochkina NE, Butikova OA. Effect of fibrous ${\rm TiO}_2$ filler on the structural, mechanical, barrier and optical characteristics of biodegradable maize starch/PVA composite films. Int J Biol Macromol. 2019;139:431–9.
- [55] Xu A, Wang Y, Gao J, Wang J. Facile fabrication of a homogeneous cellulose/polylactic acid composite film with improved biocompatibility, biodegradability and mechanical properties. Green Chem Green Chem. 2019;21:4449-56.
- [56] Yang Y, Zhang H, Wang P, Zheng Q, Li J. The influence of nanosized TiO₂ fillers on the morphologies and properties of PSF UF membrane. J Membr Sci. 2007;288:231–8.
- [57] Kumar Ashok D, Palanichamy V, Roopan SM. Photocatalytic action of AgCl nanoparticles and its antibacterial activity. J Photochem Photobiol B Biol. 2014;138:302-6.
- [58] Rajeshkumar S, Nandhini NT, Manjunath K, Sivaperumal P, Krishna Prasad G, Alotaibi SS, et al. Environment friendly synthesis copper oxide nanoparticles and its antioxidant, antibacterial activities using Seaweed (Sargassum longifolium) extract. J Mol Structure. 2021;1242:130724.
- [59] Roopan SM, Devi Priya D, Shanavas S, Acevedo R, Al-Dhabi NA, Arasu MV. CuO/C nanocomposite: synthesis and optimization using sucrose as carbon source and its antifungal activity. Mater Sci Eng C. 2019;101:404–14.
- [60] El-Sayed SM, Amer MA, Meaz TM, Deghiedy NM, El-Shershaby HA. Microstructure optimization of metal oxide nanoparticles and its antimicrobial activity. Measurement. 2020;151:107-91.